OPTICAL PROPERTIES OF POROUS ALUMINA CERAMICS WITH MICRON OPEN CELLS **

B. Liu, Ch. Sun, X. Chen, X. Xia*

School of Energy Science and Engineering, Harbin Institute of Technology, Harbin 150001, China; e-mail: xiaxl@hit.edu.cn

Porous ceramic material is widely used in a great deal of fields. In this work, porous alumina ceramics with micron open cells are modeled by applying the inverse opal structure. The considered porous alumina ceramics are periodic with different size parameters. The diameters of spherical pores are 200, 400, 600, and 800 nm, while the ratios of height to diameter range from 0.1 to 0.9. The absorptivity, transmissivity, and reflectivity for the wavelength range from 0.2 to 2 μm are calculated using the finite difference time domain (FDTD) method. Then the effects of size parameters and incident angle on the optical properties are discussed. The results show that the absorptivity is usually very small. For the transmissivity, a wide dip in the transmission spectrum appears when the diameter and height exceed the critical values, and a red shift of the transmission spectrum's wide dip with increasing height is observed. When the incident wavelength is longer than the critical wavelength, the spectral transmissivities of porous ceramics with a certain diameter reach a stable domain. Moreover, the red shift of the wide dip, the critical incident wavelength, and the critical ratio of height to diameter are visibly affected by the size parameters and the incident angle.

Keywords: *porous ceramic material, inverse opal structure, optical properties, finite difference time domain method.*

ОПТИЧЕСКИЕ СВОЙСТВА ПОРИСТОЙ АЛЮМООКСИДНОЙ КЕРАМИКИ С МИКРОННОЙ ОТКРЫТО-ЯЧЕИСТОЙ СТРУКТУРОЙ

B. Liu, Ch. Sun, X. Chen, X. Xia*

УДК 539.194

Школа энергетической науки и техники, Харбинский технологический институт, Харбин 150001, Китай; e-mail: xiaxl@hit.edu.cn

(Поступила 3 сентября 2018)

Пористая алюмооксидная керамика с микронными открытыми ячейками моделируется с помощью структуры инвертированного опала. Рассматриваемая керамика представляет собой периодическую структуру с различными геометрическими параметрами: диаметр сферических пор 200, 400, 600 и 800 нм, отношение высоты к диаметру изменяется в диапазоне 0.1–0.9. Поглощающая способность, коэффициент пропускания и отражательная способность для диапазона 0.2–2.0 мкм рассчитаны с использованием метода конечных разностей во временной области (FDTD). Обсуждается влияние геометрических параметров и угла падения на оптические свойства. Показано, что поглощающая способность обычно очень мала. Когда диаметр и высота превышают критические значения, в спектре пропускания появляется широкий провал и с увеличением высоты наблюдается его красное смещение. Когда длина падающей волны становится больше критической, спектральные коэффициенты пропускания пористой керамики с определенным диаметром достигают стабильной области. Красное смещение провала, критическая длина волны падающего излучения и критическое отношение высоты к диаметру, очевидно, зависят от геометрических параметров и угла падения.

Ключевые слова: *пористый керамический материал, структура инвертированного опала, оптические свойства, метод конечных разностей во временной области.*

** Full text is published in JAS V. 86, No. 6 (https://www.springer.com/journal/10812) and in electronic version of ZhPS V. 86, No. 6 (http://www.elibrary.ru/title_about.asp?id=7318; sales@elibrary.ru).

Introduction. Porous materials are expected to find a growing number of applications in modern development of science and engineering. Porous materials present unusual superiorities [1–3] including optical properties, low thermal conductivity, low density, high permeability and high surface area. Extensively employed porous materials include metal, polymer, and ceramic. Three-dimensionally ordered porous materials have been intensively investigated in recent decades, and their fabrication processes are rapidly developing with advanced nano-manufacturing technology [4–6]. The inverse opal structure is one of main techniques for fabrication of the three-dimensionally ordered porous materials. The sol-gel synthesis method for artificial inverse titanium opals was introduced by Wijnhoven et al. [7]. An important advantage of the inverse opals is that this kind of structure consists of an ordered arrangement of pores. As a result of periodic modulation of structures and properties, ceramics are produced with the functionality of a photonic crystal, which leads to the regulation and control of the incident radiation in certain wavelength ranges [8–10].

The mechanical, chemical, and electromagnetic properties of porous materials have been investigated in depth. Furlan et al. [11] fabricated the inverse alumina opals and tested the structural transformation under high temperatures. Bristy et al. [12] presented nanocomposite particles possessing superparamagnetic properties in porous γ-Al_2O_3 ceramics by applying X-ray photoelectron spectroscopy. Shi et al. [13] demonstrated a possible phase transition of α-Al_2O_3 powder and microstructural transformation inside porous ceramic materials. Bakken et al. [14] reported the biaxial strength and subcritical crack growth of three porous alumina ceramics prepared by using coarse grained alumina powder and silica as sintering aid. In the fields of catalysts [15], photonic crystals [16, 17], and other application in thermology and optics, the interactions of light and porous materials are vital and influential for further researches. For the optical and radiative properties of porous material, some excellent works have appecued. Contento et al. [18] proposed a theoretical approach to develop a new radiative heat transfer model based on the tetrakaidecahedron representation of open cell metal foams and evaluated the radiative conductivity of foams by means of the proposed model. Martin et al. [19] reported on the fabrication and characterization of tungsten inverse opals for the visible and near-infrared spectral region and investigated experimentally the crucial influence of the strong absorption in this spectral region by means of the gradient deposition technique. Braun et al. [20] performed some experiments to discuss the reflectivity of nickel inverse opals at the wavelength range of 1.5–5.5 μm. Yeng et al. [21] studied the emittance of a two-dimensional tungsten photonic crystal, which consists of an array of cylindrical cavities at different high temperatures and experimentally obtained thermal emissivity spectra that match well with numerical simulations. Liu et al. [22] investigated theoretically the spectral radiative properties of a kind of nickel porous microstructure, including wavelength-selective transmission, reflection, and absorption. These works mostly focus on porous material made of metal and polymer.

Comparing with metals and polymers, porous ceramic materials have longer lifetimes, constant filter quality, and thermal stability [23–25]. Therefore, the materials are widely used in filters, catalysts support, bioreactors, thermal insulators, sensors, and bone substitutes [26–28]. Kapitonov et al. [29] examined the optical transmission spectra of a SiO_2/TiO_2 three-dimensional cubic lattice. Kubrin et al. [30] investigated the feasibility of stacking of thin ceramic inverse opals with incommensurable periodicity constants, and conducted experiments for TiO_2 inverse opals. Guan et al. [31] studied the fabrication and structural analysis of three-dimensionally well-ordered arrangements of silicon oxycarbide microparticles. However, research on the optical properties of porous ceramic materials has not attracted enough attention. Besides, the alumina porous ceramics, one of the most widely used hard ceramic oxides possessing properties like thermal stability [32], high dielectric constant [33, 34], and advanced application for bioceramics [35, 36] have been studied less.

In this work, the three-dimensionally ordered porous ceramics made of alumina are modeled by applying the inverse opal structure. The optical properties are predicted by applying the FDTD method. The modeling process of the three-dimensionally ordered porous ceramics is introduced. The method and calculating conditions are presented. In the following section, the results of optical properties are discussed.

Geometric model and numerical method. Porous material with the inverse opal structure. The 3D porous materials are usually made up of micro-scaled structures, and the sizes of these detailed structures are similar to the wavelength of light. The inverse opal structure is one of the representative manufacturing processes for micro-scaled porous material. The inverse opal structure could be produced only in the voids between adapted templates.

In this work, the inverse opal structures made of alumina ceramics are modeled by simulating the manufacturing processes. The detailed processes are shown in Fig. 1. The porous ceramics is characterized by two

size parameters, including the diameter *d* of spherical templates and the height of the inverse opal structures *h* as shown in Figs. 1a,d.

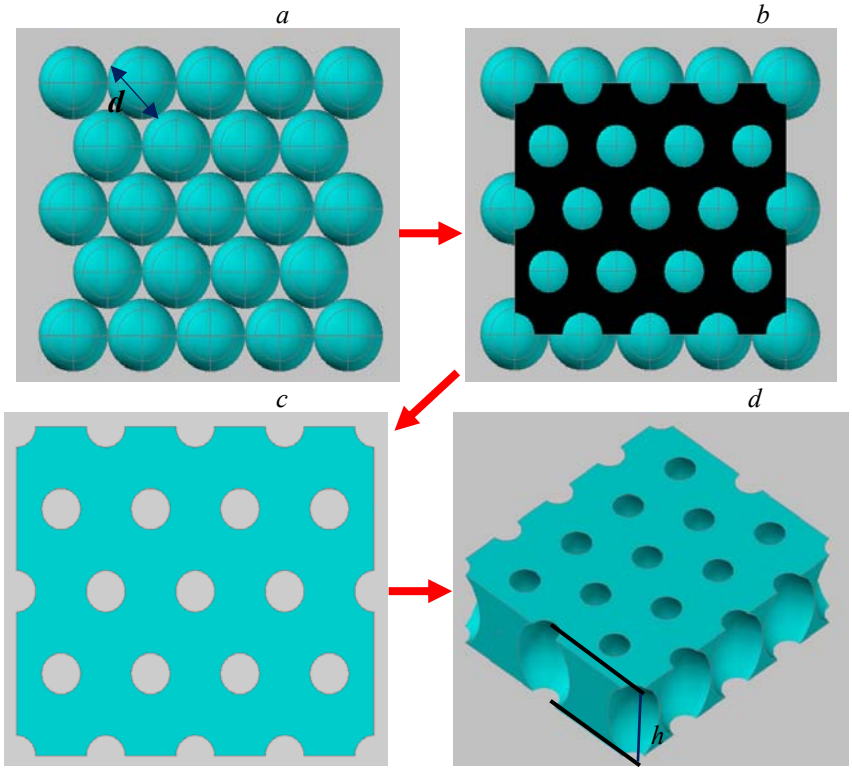

Fig. 1. The modeling process for the inverse opal structure: (a) is the colloidal crystals that self-assembled into a closely packed structure with 3D ordered lattices. These spheres are the templates for later process; (b) is the state after filling molten alumina ceramics. The square part represents the molten alumina ceramics surrounding the spheres; (c) is the resulting structures after removing the templates and solidification of fluid; (d) are a three-dimensional view of the modeled inverse opal structure.

Many excellent works on the fabrication and properties of three-dimensional periodic porous material have been presented. In these researches, the diameters of adapted spherical templates range from 200 to 800 nm as shown in [11, 30, 31], while the heights are usually decided by different applications and designs. After summarizing and analyzing the size characteristics of the inverse opal structures, we note that the studied opal structures in this work have diameters of 200, 400, 600, and 800 nm. For convenience of expression, the height of the inverse opal structure is characterized by the ratio of height *h* to diameter *d*. The ratios *h*/*d* considered here range from 0.1 to 0.9, which can show the radiative properties with changing height adequately. The discussed material is alumina, and the spectral complex refractive index of alumina adapted here are from [37].

From the inverse opal structure shown in Fig. 1d, we see that the whole structure is periodic and symmetric. The representative elements having enough micron cells are chosen for subsequent calculation of optical properties. The three-dimensional computational domain is set as follows. The top and bottom of the domain are considered as boundary conditions with a perfectly matched layer (PML). When the direction of light is normal to the upper surface of the inverse opal microstructure, the sides around the structure computational domain are treated as periodic boundary conditions. When the direction of light is oblique to the upper surface of the structure, the sides around the structure computational domain are treated as Bloch boundary conditions. In this work, the discussed problems are under nonpolarized light. The final results are the mean values of corresponding predicted parameters for two kinds of polarizations.

The FDTD method. In recent decades, methods of numerical calculation for solving micro-scaled radiation problems have been developing rapidly. Many methods, such as the method of moments, the finite element method, and others, have been applied in various fields. The finite difference time domain [38] (FDTD) method used in this work is one of the main methods for computational electromagnetism, and it has been

improved completely since the method was presented by Yee. The work here for the prediction of optical parameters of the inverse opal structures is based on the FDTD method. For the nonmagnetic material, the Maxwell equations and constitutive equation are as followed:

$$\nabla\times\mathbf{H} = \partial\mathbf{D}/\partial t, \tag{1}$$

$$\nabla\times\mathbf{E} = -\mu_0\partial\mathbf{H}/\partial t, \tag{2}$$

$$D = \varepsilon_0\varepsilon_r E, \tag{3}$$

where **H**, **E**, and **D** are the magnetic field, the electric field and the electric displacement vector, respectively, μ_0 is the permeability of vacuum, and ε_0 and ε_r are the permittivity of vacuum and relative permittivity. The time-averaged power flow across a surface is defined by

$$P = \int_a Sds = \int_a \frac{1}{2}\mathrm{Re}[\mathbf{E}\times\mathbf{H}^*]ds, \tag{4}$$

where $\mathbf{H}^*$ is the complex conjugate of the magnetic field vector, and a is the area of the surface used to monitor the power flux. In this work, the reflectivity and bidirectional reflectance distribution function (BRDF) are discussed. The reflectivity R and transmissivity T is defined by

$$R = P_R/P_i, \tag{5}$$

$$T = P_T/P_i, \tag{6}$$

where P_R is the power of reflected light, P_i is the power of incident light, and P_T is the power of transmitted light. Furthermore, the absorption A will be obtained by the formula $A = 1 - R - T$.

For verifying the accuracy and validity of the FDTD method adapted in this work, the absorptivity of tungsten grating calculated by the rigorous coupled wave analysis (RCWA) in [39] is calculated again by applying the adapted FDTD method. The grating has periodic length 1.6 μm, height 0.2 μm and width 1.28 μm. The results predicted by the FDTD method here are compared with the calculated results in [39]. Moreover, the reflectivity of the nickel porous material in [22] is calculated again. The nickel porous material is also produced by applying the inverse opal structure, which has a diameter of 0.2 μm and a height of 0.175 μm. From the comparison, the FDTD method used in this work is reliable for the prediction of optical properties of the discussed structures.

Results and discussion. The diameters of spherical pores are 200, 400, 600, and 800 nm, and the ratios of height to diameter range from 0.1 to 0.9. The incident wavelengths range from 0.2 to 2 μm, which includes the visible and near infrared band for spectral calculations. According to the grid independence test, a mesh size of λ/80 is used in this paper. The reflectivities, absorptivities, and transmissivities of different structures with various size parameters are predicted and compared. Furthermore, the effects of the size parameters and incident angle on the optical properties are discussed and analyzed.

The characteristics of optical properties. Taking a comprehensive consideration of all the cases discussed here, the behaviors of optical properties show great consistency. Among all the cases, the transmission, reflection, and absorption spectra of the porous ceramics with diameters of 600 nm show all the main variation characteristics of optical properties discussed in this work at the band from 0.2 to 2 μm. The spectral reflectivities, absorptivities, and transmissivities of the porous ceramics with d = 600 nm are depicted in Fig. 2. In Fig. 2a, the spectral absorptivities of porous ceramics are shown. For an incident wavelength of 0.2 μm, the absorptivity increases gradually with increasing height h. For the condition of h/d = 0.1, the absorptivity is close to zero. For a longer wavelength, the absorptivity decreases rapidly. The change of the absorption spectra is due to a rapid decrease of the imaginary part of complex refraction k. The absorptivities under longer wavelengths tend to zero. The transmissivity T is shown in Fig. 2b. The optical properties of the porous ceramic material show obvious spectral selectivity. When h/d < 0.6, the transmissivity increases with growing incident wavelengths, but the increase gradually slows down and then remains in the stable domain shown in Fig. 2b. In the stable domain, the values of transmissivity are bigger than 0.95 and change slightly. When h/d > 0.6, a wide dip appears in the transmission spectra. Locations of the wide dip move to a longer wavelength with increasing h/d, which means a red shift of the wide dip exits with increasing h/d when h/d exceed 0.6. The critical value of h/d for the wide dip appearance is called 'the first critical value' in this work, and the first critical value of the case with d = 600 nm is 0.6. When the wavelength exceeds 1.6 μm, the transmissivities of all the cases with different h/d reach the stable domain where the transmissivities of all the cases hold around a stable value above 0.95. There is a critical value of the incident wavelength after which all transmissivities change hardly. This critical wavelength is called 'the second critical value', and the second critical value of the case with d = 600 nm is 1.6. Figure 2c is the reflectivities of the cases

discussed here. The reflectivity variation curves are closely mirror to the variation curves of transmissivity shown in Fig. 2b. Absorptivity is small compared with the transmissivity and reflectivity.

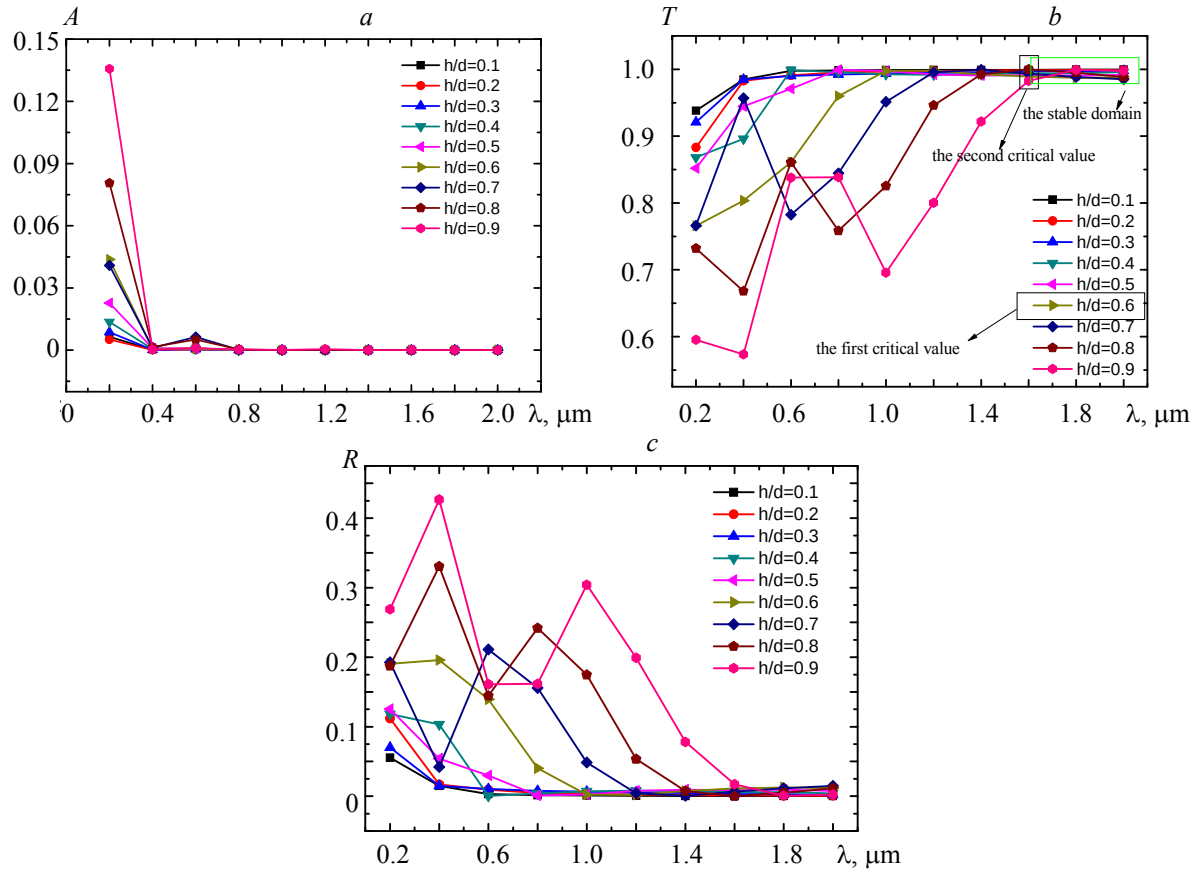

Fig. 2. The spectral radiative properties of the porous ceramics with d = 600 nm: the absorptivity A (a), transmissivity T (b), and reflectivity R (c).

The influence of size parameters on the spectral transmissivity. The effect of size parameters and incident angle on the optical properties is analyzed. From the discussion above, the absorptivities are very small compared with the transmissivities and reflectivities, and the shape of the reflectance curve is close to mirror-symmetric as compared with the shape of the transmittance curve. Thus, the transmissivity of porous ceramics will be discussed only.

Figure 3 depicts the transmissivities of porous alumina ceramics with different diameters. From the transmissivities of porous alumina ceramics with diameter of 200 nm, as shown in Fig. 3a, the transmissivities of all the cases here increase with growing wavelength first, and then hold around a stable value above 0.95. Wide dips are absent, and thus the red shift of the wide dip does not exit. For the cases of d = 400, 600, and 800 nm (Fig. 3b–d) the wide dips exit at different locations. The red shift of the wide dip becomes more and more obvious when the diameters of pores grow larger overall. The two critical values discussed above are also compared here. There are no first critical values of the porous ceramics with d = 200 nm because the wide dip does not exit. For the porous ceramics with diameters of 400, 600, and 800 nm, the corresponding first critical values are 0.6, 0.6, and 0.2, respectively. Hence, one can see that the first value of the porous ceramic material with micron open cells changes with increasing diameters. The second critical values can be observed in the pictures of transmissivities of the porous ceramics with diameters of 200, 400, and 600 nm, while the second critical values of the porous ceramics with different diameters are 0.6, 1.2, and 1.6, respectively. For the cases with d = 800 nm, the transmissivities of all the cases have not reached the stable domain when the incident wavelength becomes 2 μm, but the second critical value of the porous ceramics

with d = 800 nm can be forecasted to be a value exceeding 2. Thus, the second critical value of the porous ceramics with micron open cells increases with growing diameters.

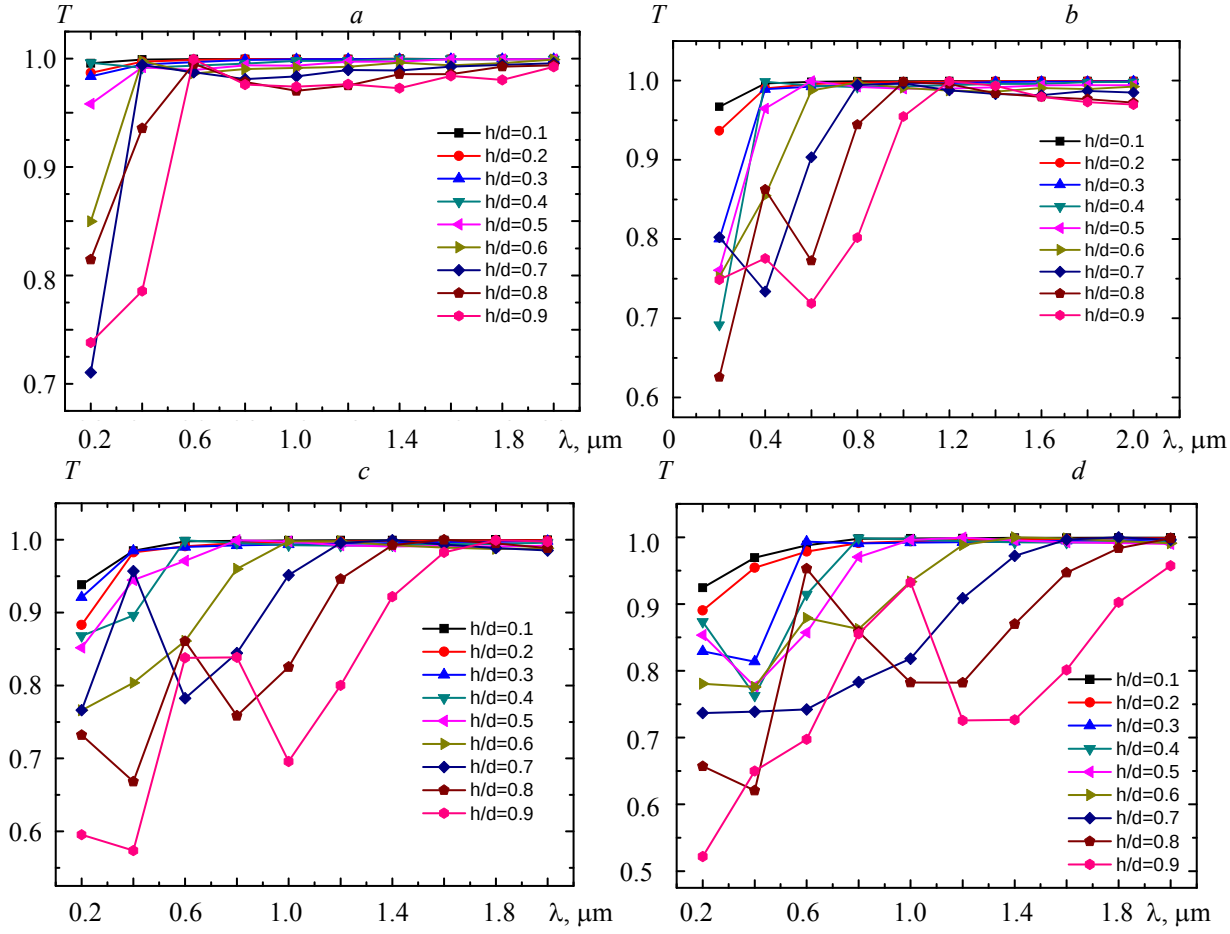

Fig. 3. The transmissivity of the porous alumina ceramics with the pore diameter d = 200 (a), 400 (b), 600 (c), and 800 nm (d).

The effects of incident angle on the spectral transmissivity. From the discussion above, the optical properties of the porous alumina ceramics with micron open cells are affected by the increasing size parameters. Another influencing factor of the optical properties is the incident angle. The effects of the incident angle on the optical parameters are shown in Fig. 4, where the results are based on the structures with d = 600 nm and h/d ranging from 0.1 to 0.9. From Fig. 4, there are wide dips in the transmission spectra for all the porous ceramics under different incident angles when h/d exceeds the first critical values. By comparing the results shown in Fig. 4, locations of the wide dips under normal incidence are separated completely, while the locations become nearer under the incident angle of 30°. When the incident angle is 60°, the locations are the same. Hence it can be seen that the red shift of the wide dip is weakened by growing incident angle and even vanishes completely when the incident angle is large enough. For the porous ceramics under the incident angle of 0, 30, and 60°, the corresponding first critical values are 0.6, 0.5, and 0.2. Thus, the first critical value decreases with increasing incident angle. The second critical values of the porous ceramics under the incident angles of 0, 30, and 60° are 1.6, 1.4, and 0.6, respectively. This shows that the second critical value decreases with growing incident angle, too.

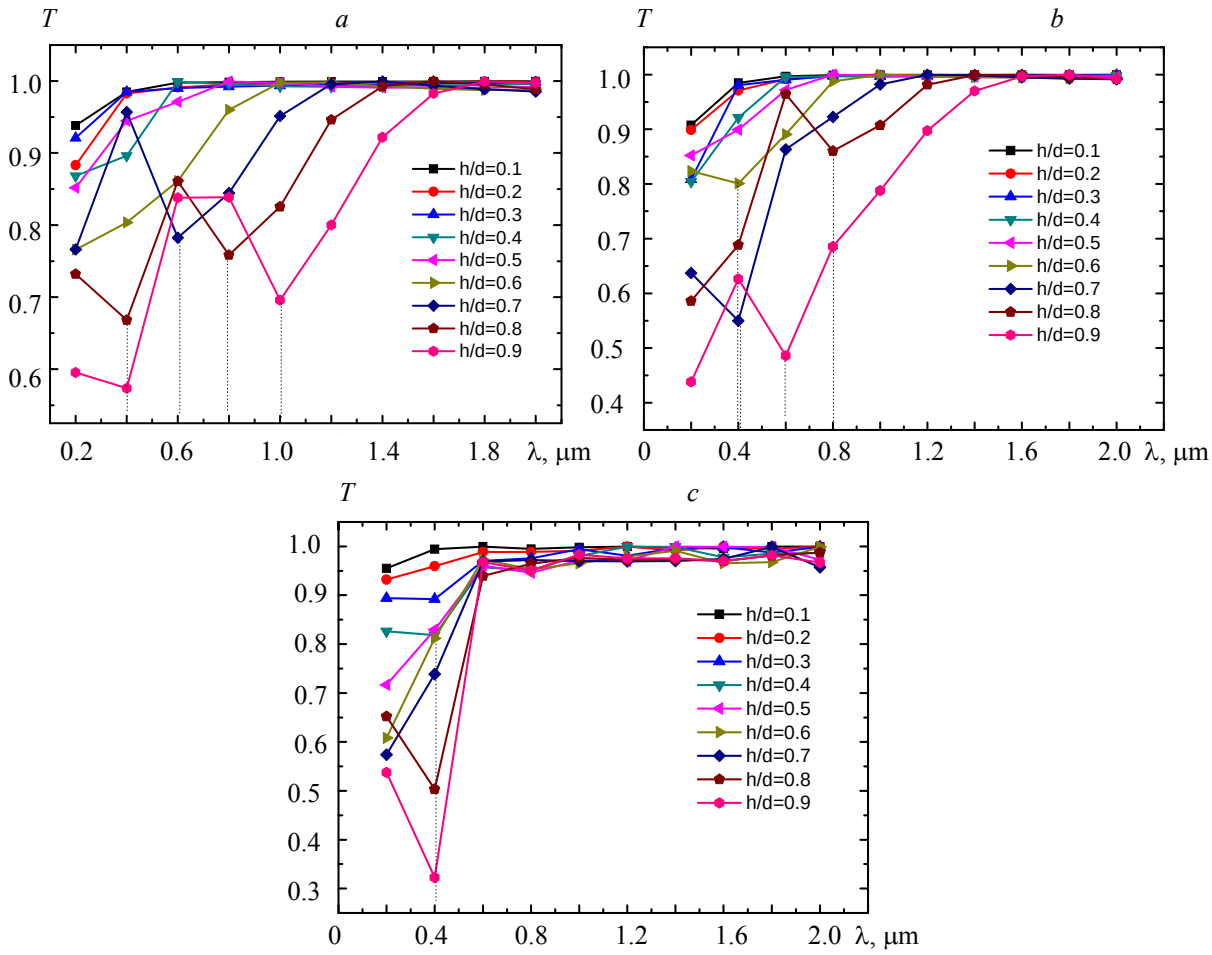

Fig. 4. The transmissivity of the porous alumina ceramics under different incident angles: normal incidence (a), 30° (b), and 60° (c).

Conclusion. The inverse opal structures with different size parameters are applied to model the porous alumina ceramic material with micron open cells. The optical properties of porous ceramics including absorptivity, reflectivity and transmissivity are calculated and analyzed by applying the FDTD method. The effects of size parameters and incident angle on the optical properties are discussed. There are several conclusions that can be summarized as following. 1) For the modeled porous alumina ceramics, absorptivity is usually very small and reflectivity shows opposite variation regulation compared with transmissivity. There are two critical values for the spectral transmissivity of porous ceramics with certain diameter and various heights. The wide dip in the transmission spectrum exits when the diameter is not less than 400 nm and the value of h/d is larger than the first critical value, and the red shift is observed. Transmissivity in all the cases with a certain diameter reaches the stable domain when the incident wavelength exceeds the second critical value. 2) Optical properties of the porous alumina ceramics with micron open cells are affected by increasing size parameter. The red shift of the wide dip becomes more and more obvious when the diameter of pores grows larger overall. The critical value for the ratio of height to diameter changes with increasing diameters, while the critical value of incident wavelength increases with growing diameters. 3) The red shift of the wide dip is weakened by growing incident angle and even vanishes completely when the incident angle is large enough. The critical height and critical incident wavelength both decrease with increasing the incident angle.

Acknowledgment. The work is supported by the National Natural Science Foundation of China (No. 51536001) and National Natural Science Foundation of China (No. 51776053).

REFERENCES

1. G. Subramania, K. Constant, R. Biswas, M. M. Sigalas, K. M. Ho, *Appl. Phys. Lett.*, **74**, 3933–3935 (1999).
2. A. Richel, N. P. Johnson, D. W. Mccomb, *Appl. Phys. Lett.*, **76**, 1816–1818 (2000).
3. H. Míguez, F. Meseguer, C. López, F. López-Tejeira, J. Sánchez-Dehesa, *Adv. Mater*., **13**, 393–396 (2001).
4. Daimu Muto, Shinobu Hashimoto, Sawao Honda, Yusuke Daiko, Yuji Iwamoto, *Ceram. Int.*, **44**, 3678–3683 (2017).
5. H. Asoh, A. Uehara, S. Ono, *Jpn. J. Appl. Phys.*, **43**, L1159–L1161 (2014).
6. J. E. G. J. Wijnhoven, L. Bechger, W. L. Vos, *Chem. Mater.*, **13**, 4486–4499 (2001).
7. J. E. G. J. Wijnhoven, W. L. Vos, *Science*, **281**, 802–804 (1998).
8. A. A. Miskevich, V. A. Loiko, *J. Quant. Spectrosc. Radiat. Transf*., **151**, 260–268 (2015).
9. A. A. Miskevich, V. A. Loiko, *J. Quant. Spectrosc. Radiat. Transf*., **112**, 1082–1089 (2011).
10. V. A. Loiko, A. A. Miskevich, *Opt. Spectrosc.*, **122**, 799–812 (2017).
11. K. P. Furlan, R. M. Pasquarelli, T. Krekeler, M. Ritterb, R. Zieroldc, K. Nielschc, G. A. Schneidera, R. Janssen, *Ceram. Int.*, **43**, 11260–11264 (2017).
12. S. S. Bristy, M. A. Rahman, K. Tauer, H. Minamic, H. Ahmad, *Ceram. Int.*, **44**, 3951–3959 (2018).
13. Ruixia Shi, Yaru Shang, Yan Zhang, Peng Wang, Aiyu Zhang, Ping Yang, *Ceram. Int.*, **44**, 3741–3750 (2017)
14. A. Bakken, S. Wagner, M. J. Hoffmann, B. Thorstensen, M. A. Einarsrud, T. Grande, *J. Eur. Ceram. Soc.*, **38**, 665–670 (2017).
15. Xiaoyun Song, Qingxin Guan, Zitao Cheng, Wei Li, *Appl. Catal. B: Environ.*, **227**, 13–23 (2018).
16. M. Gallei, *Macromol. Rapid. Commun.*, **39**, 1700648 (2017).
17. A. A. Miskevich, V. A. Loiko, *J. Exp. Theor. Phys.*, **113**, 1 (2011).
18. G. Contento, M. Oliviero, N. Bianco, V. Naso, *Int. J. Heat Mass Transf.*, **76**, 499–508 (2014).
19. G. Von Freymann, S. John, M. Schulz-Dobrick, E. Vekris, N. Tétreault, S. Wong, V. Kitave, G. A. Ozin, *Appl. Phys. Lett*., **84**, 224–226 (2004).
20. X. Yu, Y. J. Lee, R. Furstenberg, J. O. White, P. V. Braun, *Adv. Mater.*, **19**, 1689–1692 (2007).
21. Y. X. Yeng, M. Ghebrebrhan, P. Bermel, W. R. Chan, J. D. Joannopoulos, M. Soljacic, I. Celanovic, *Proc. Natl. Acad. Sci.*, **109**, 2280–2285 (2012).
22. Y. B. Liu, R. Jin, J. Qiu, L. H. Liu, *Int. J. Heat Mass Transf.*, **98**, 833–844 (2016).
23. Z. Chen, N. Brandon, *Ceram. Int.*, **42**, 8316–8324 (2016).
24. V. A. Loiko, A. A. Miskevich, *Opt. Spectrosc.*, **115**, 274–282 (2013).
25. A. A. Miskevich, V. A. Loiko, *J. Quant. Spectrosc. Radiat. Transf*., **136**, 58–70 (2014).
26. R. Liu, Y. Li, C. A. Wang, S. Tie, *Mater. Design.*, **63**, 1–5 (2014).
27. F. Tian, L. Jing, J. Shi, M. Yang, *Sensor. Actuator. B: Chem.*, **225**, 312–318 (2016).
28. S. Li, C. A. Wang, J. Zhou, *Ceram. Int.*, **39**, 8833–8839 (2013).
29. A. M. Kapitonov, N. V. Gaponenko, V. N. Bogomolov, A. V. Prokofiev, S. M. Samoilovich, S. V. Gaponenko, *Phys. Status Solidi (A)*, **165**, 119–123 (1998).
30. R. Kubrin, H. S. Lee, R. Zierold, A. Yu. Petrov, R. Janssen, K. Nielsch, M. Eich, G. A. Schneide, *J. Am. Ceram. Soc.*, **95**, 2226–2235 (2012).
31. G. Guan, K. Kusakabe, H. Ozono, M. Taneda, M. Uehara, H. Maeda, *Chem. Eng. J.*, **135**, 232–237 (2008).
32. M. Munro, *J. Am. Ceram. Soc.*, **80**, 1919–1928 (1997).
33. S. Mallakpour, M. Dinari, *Mater. Res. Bull.,* **48**, 3865–3872 (2013).
34. K. Noh, K. S. Brammer, T. Y. Seong, S. Jin, *Nano*, **06**, 541–555 (2011).
35. M. Cárdenas, T. Arnebrant, A. Rennie, G. Fragneto, R. K. Thomas, L. Lindh, *Biomacromolecules*, **8**, 65–69 (2007).
36. I. Vlassiouk, A. Krasnoslobodtsev, S. Smirnov, M. Germann, *Langmuir*, 2004, **20**, 9913–9915 (2004).
37. E. D. Palik, *Handbook of Optical Constants of Solids*, Academic Press, Orlando (1985).
38. K. S. Yee, *IEEE Trans. Anten. Propag.*, **14**, 302–307 (1966).
39. Y. B. Chen, Z. M. Zhang, *Opt. Commun.*, **269**, 411–417 (2007).